Towards an Active Optical Clock using an Optical Conveyor within a Ring Cavity

Kazakov G*., Dubey S.
Atominstitut, TU Wien
Vienna, Austria
*georgy.kazakov@tuwien.ac.at

Famà F., Zhou S., Beli Silva C., Schäffer S.A.,
Bennetts S., Schreck F.
Van der Waals - Zeeman Institute, Institute of Physics,
University of Amsterdam,
Amsterdam, the Netherlands
iqclock@strontiumbec.com

***Abstract* — We report on our progress towards a continuously-operating active optical clock on the $^3P_0 \rightarrow {}^1S_0$ transition of neutral ^{87}Sr or ^{88}Sr atoms. Our approach is based on a ring-cavity in which an optical conveyor carries a continuous stream of atoms along the cavity mode. We estimate the performance of our system by simulating the superradiant output from two counter-propagating cavity modes interacting with the atoms. The impact of the position-dependent light shifts, collisional decoherence and loss of atoms trapped within the optical conveyor are analysed.**

Keywords — active optical clocks, optical conveyor, ring cavity, Strontium, calculation

I. INTRODUCTION

In a passive optical atomic clock the frequency of a laser is intermittently compared with a narrow *clock transition* in a sample of trapped atoms or ions. In between frequency comparisons this laser must be stabilized by locking it to a mode of a high finesse, ultrastable, macroscopic, reference cavity. Such clocks have demonstrated excellent stability reaching 6.6 x 10^{-19} after 1 hour of averaging [1]. However, on short timescales this stability remains limited by factors such as environmental and thermal fluctuations impacting the reference cavity length. This problem may be overcome with the help of a superradiant laser operating in a so-called *bad-cavity regime,* where the linewidth of the cavity is much broader than the gain profile. The frequency of such a laser is inherently insensitive to cavity perturbations making the output frequency robust also on short timescales. This opens a possibility to create an active optical frequency standard [2,3], similar to the hydrogen maser, but operating in the optical domain. Here the gain is provided by forbidden transitions in alkaline-earth atoms confined in a magic optical lattice potential. The first steps have already been taken with pulsed bad-cavity lasing on the $^3P_0 \rightarrow {}^1S_0$ transition observed from neutral ^{87}Sr atoms at JILA, USA [4]. Here we discuss our approach towards demonstrating a continuously-operating device.

II. EXPERIMENTAL SETUP

A continuously-operating bad-cavity laser is necessary for creating an active clock or frequency standard. This requires continuously replenishing the atoms. Such replenishing can be realised with the help of an optical conveyor continuously delivering atoms in the excited $^3P_0$ state to the active zone [5]. Realisation of this scheme becomes possible with the creation of a continuous source of guided ultracold Sr atoms, able to deliver several tens of millions of ^{88}Sr, or several millions of ^{87}Sr atoms per second [6-8].

An optical conveyor confining atoms may cross the optical lattice created within a standing-wave cavity as shown in figure 1 (a). It is necessary to keep the atom-cavity interaction time long in order to reach the superradiant laser threshold and efficiently extract signal from the atoms. Therefore one needs to pull the atoms through the cavity relatively slowly, and a significant portion of the atoms will be lost from the conveyor before they reach the cavity. Also, the high density of the atoms within the cavity may cause undesirable density-related effects. Another approach is to create an optical conveyor carrying atoms along a ring cavity as shown in figure 1 (b). This allows extremely long atom-cavity interaction times while keeping the density of the atoms low by increasing the conveyor speed. However, one must stabilize parameters affecting the atoms over larger spatial volumes. Such an approach is investigated here, and also used in [9].

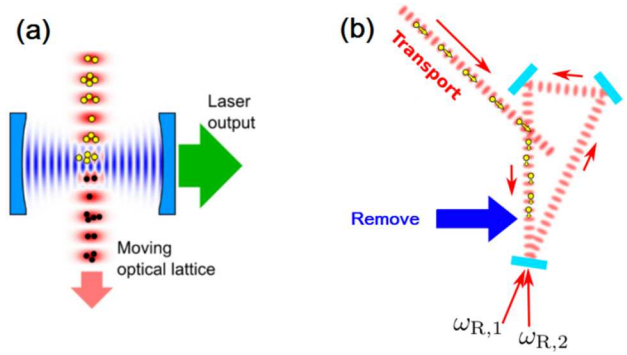

Fig. 1 Schematics of bad-cavity lasers with (a): optical conveyor crossing the standing-wave optical cavity, and (**b**) optical conveyor excited inside the running-wave optical cavity.

978-1-6654-3935-0/21/$31.00 ©2021 European Union

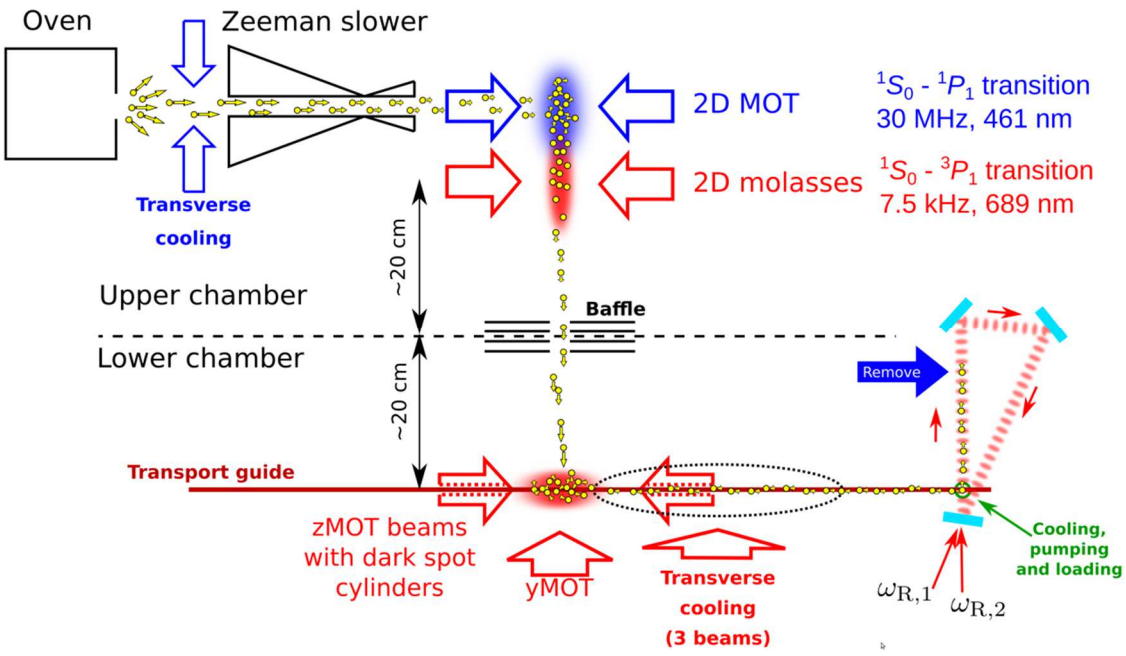

Fig. 2. Schematic of the experimental setup to cool and trap the atoms and deliver them into optical conveyor inside a ring cavity. Initially the atoms coming from an oven are slowed down by a Zeeman slower operating on 30 MHz-wide 461 nm (blue) transition. Then the atoms are gathered in a 2D magneto-optical trap (MOT), and further cooled down by 2D molasses operating on the 7.5 kHz-wide 689 nm (red) transition located directly below the blue MOT. Then the atoms are transferred through the baffle into the lower chamber, where they are trapped in a 3D red MOT. Two beams forming this MOT are hollow, and they don't trap the atoms in z-direction near the axis of the red MOT. A transport guide beam (1070 nm) passes through these dark spot cylinders to confine the atoms along the *x* and *y* axis. Then the atoms are further cooled and loaded into the conveyor.

A crucial part of our setup is a continuous source of cold atoms [6-8]. This produces a guided beam of ^{88}Sr with transversal temperatures below 1 μK and a flux of 3×10^7 ^{88}Sr/s [7]. Similarly, we have demonstrated a continuously-loaded MOT of ^{87}Sr with a loading rate of 1.3×10^7 ^{87}Sr/s [8]. Our approach is based on flying Sr atoms through a series of spatially distributed laser cooling and guiding stages until they reach the microkelvin regime, see Figure 2. To protect atoms from scattering the 461-nm "blue" photons which are necessary to efficiently trap and cool hot atoms leaving the oven, a multi-chamber design is used. This isolates Sr atoms in the last cooling stages as well as those in the superradiant clock cavity.

III. SIMULATION OF THE SIGNAL

We have simulated the superradiant output signal from atoms travelling in an optical conveyor along a running-wave optical cavity. Here we present a semiclassical model analysing the impact of real-life effects, particularly from density shifts, decoherences and losses, as well as from the inhomogeneity of external magnetic fields.

In our simulations we assume a total cavity length L_c = 11 cm and a cavity finesse $F = 5 \times 10^4$, which corresponds to a cavity decay rate $\kappa = 2\pi \times 54$ kHz. We suppose that the atoms travel along the cavity over l_{conv} = 2 cm, that the cavity mode is co-propagating with the atoms and that the cavity mode is polarized along the direction of the bias static magnetic field $\underline{B}$ (which is orthogonal to the axis of the conveyor). This mode is resonant with the unperturbed $^3P_0 \rightarrow {}^1S_0$ transition in the atoms, or close to this resonance, with a frequency detuning δ. In early variants of our simulation we also included the counter-propagating off-resonant mode. However, this mode is never excited in our simulation, and we can consider a simplified model with only a single resonant mode. We suppose also that the temperature of the atoms T = 5 μK and the waist of the 698 nm cavity mode W_0 = 150 μm. The conveyor is formed by two "magic" wavelength counter-propagating waves about 813 nm with slightly different frequencies, and a potential depth of 200 recoil energies. Temperature and depth are necessary to calculate the corrected coefficients g of atom-cavity coupling, and to estimate average density of the atoms, in order to take into account density effects.

A. Simulation results for ^{88}Sr: position-dependent shifts

Single-photon $^3P_0 \rightarrow {}^1S_0$ transitions in isolated bosonic Sr are forbidden to all orders of multipole expansion. This transition might be made slightly allowed in the presence of an external field, for example, a static magnetic field [10], mixing the $^3P_0$. and $^3P_1$, m = 0 states. Such a field not only opens this transition, but also shifts the position of the new $^3P_0$ state by a second-order Zeeman shift $\delta\omega_{3P0-1S0}$ related to the induced E1 transition rate $\gamma_{3P0-1S0}$ as

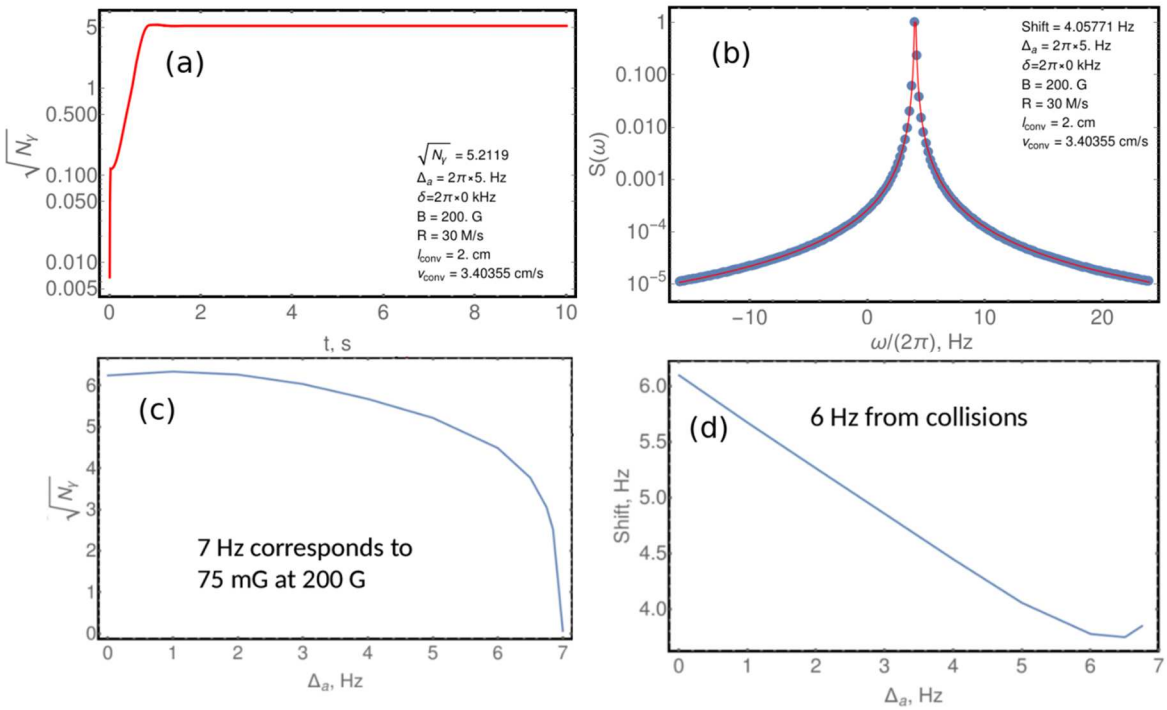

Fig. 3. Examples of simulated signals in time (a) and frequency (b) domains. (c): amplitude of intracavity field, and (d): frequency shift of the superradiant radiation with respect to the unperturbed atomic transition as a function of the amplitude of the position-dependent shift.

$$\delta\omega_{3P0-1S0} = \gamma_{3P0\to1S0}\frac{\omega_{3P1}-\omega_{3P0}}{\gamma_{3P1\to1S0}} = \beta B^2 \qquad (1)$$

where $\beta \approx -2\pi\cdot 23.3$ MHz/T^2≈ -1.464 s^{-1}/G^2 [10]. The sensitivity of the clock transition frequency to variations in the bias field thus scales with the square of the external bias field strength. This leads to considerable sensitivity in the clock transition to magnetic field fluctuations for practical bias field strengths. For an external bias field of 200G corresponding to a ^{1}S$_0$-^{3}P$_0$ transition linewidth $\gamma_{3P0-1S0}$ of just $2\pi\times 12$ μHz the second order differential Zeeman shift is already 93 mHz/mG.

Another issue related to the density is that identical bosons interact with each other via s-wave collisions. This leads to potentially large shifts and decoherences.

In this paper, we have used mean-field equations, in which we neglect quantum correlations between different atoms, and where we suppose that each atom interacts with the mean field created by all the other atoms. We have also taken into account collisional decoherence, shifts and losses, which have been adopted from [11]. To reduce computational costs, we grouped the atoms into clusters.

In Figure 3 we present some results for one of the simplest possible models of position-dependent shift, namely, a linear gradient, where the magnetic shift Δ_m of the lasing transition depends on the position z of the atom along the optical conveyor as

$$\Delta_m(z) = \Delta_a\frac{2l_{conv}-z}{l}. \qquad (2)$$

Here z lies between 0 and l_{conv}. We have taken total magnetic field $B = 200$ G, total atomic flux $R = 3\times10^7$ atoms/s, and speed of conveyor $v_{conv} \approx 3.4$cm/s. In Figures 3 (a) and (b) we present examples of simulated signals in both time- and frequency domains. Figures 3 (c) and (d) present the absolute value of steady-state intracavity field (in the semiclassical approximation this is just a square root of number of photons) and the frequency shift of the superradiant signal as a function of the amplitude Δ_a of this position-dependent shift. For our parameters the signal vanishes when $\Delta_a \approx 7$ Hz, which corresponds to approximately 75 mG of inhomogeneity in the magnetic field. The non-zero shift at $\Delta_a = 0$ is caused by collisions, see Figure 3 (d).

B. Simulation results for ^{87}Sr: lasing on stretched states

The nucleus of ^{87}Sr has a non-zero magnetic moment and a total spin I = 9/2. Hyperfine interaction between the nuclear and electronic moments leads to a mixing of the ^{3}P$_0$ and ^{3}P$_1$ states. Therefore, single-photon ^{3}P$_0\to{}^1$S$_0$ transitions are slightly allowed in fermionic Sr, and there is no need for a strong external magnetic field. A weak (~1G) magnetic field is used to lift degeneracy preventing the emergence of non-desirable coherent effects between different Zeeman substates of the upper- and the lower lasing states. The differential Zeeman shift between Zeeman sublevels of the ^{3}P$_0$ and ^{1}S$_0$ states with equal projection m of the total momentum onto the quantization axis is equal to $(2\pi\times 108.4)$ Hz/G $\times\, m \times B$ [12]. The atoms can be pumped into the stretched states with $m = \pm 9/2$. The bad-cavity laser may operate on both of these transitions simultaneously, see Figure 4 (a).

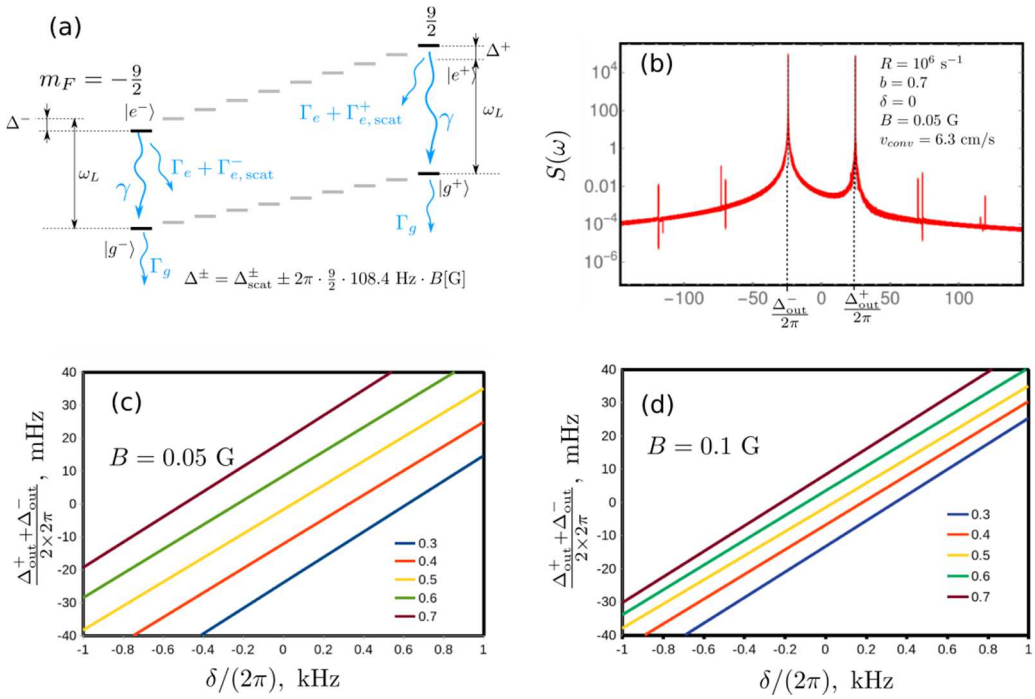

Fig. 4. (a) Zeeman structure of the $^1S_0$ and $^3P_0$ states of ^{87}Sr and stretched transitions. (b): example of a simulated spectrum from the superradianl laser. Here the cavity is in resonance with unperturbed $^1S_0$ --- $^3P_0$ transition of ^{87}Sr in the absence of any magnetic field, R is the rate of atoms loaded into the conveyor, b is a balance parameter, see eq. (3), B is the static magnetic field. (c) and (d): dependence of the non-weighted arithmetic mean of two output frequencies on the cavity detuning for different values of parameter b (given in legend) at B = 0.05 G (c) and B = 0.1 G (d)

If the magnetic field B is weak, the Zeeman splitting between two stretched states will be small, and the lasing process on both of these stretched transitions will synchronize. The output radiation will have a single frequency in such a case. However, the frequency of this mode depends on the distribution of the atoms over the different stretched states, and this imbalance will shift the line. It is convenient to introduce a balance parameter b as

$$b = \frac{P_{-9/2}}{P_{-9/2}+P_{9/2}}, \qquad (3)$$

where $P_{\pm 9/2}$ is the number of atoms pumped into the stretched state with $m = \pm 9/2$ respectively. The frequency of the superradiant line will depend on this balance parameter b.

At larger values of Zeeman splitting the lasing processes on the stretched transitions will not be synchronized, and the output radiation will have two frequencies $\omega^{\pm}_{out}$ shifted from the frequency of the unperturbed $^3P_0 \rightarrow {}^1S_0$ transition by $\Delta^{\pm}_{out}$ respectively, see Figure 4 (b). We present an example simulated spectrum of two-frequency radiation at B = 0.05 G. Each of these frequencies will be primarily determined by the frequency of the respective stretched transition and its perturbation. Any fluctuations in the static magnetic field will cause opposite first-order Zeeman shifts of these stretched transitions, thus, the non-weighted arithmetic mean $\omega_{out} =$ of these frequencies will be immune to these fluctuations up to the second-order Zeeman effect. However, some interaction between different stretched transitions remains at moderate values of Zeeman splitting. In Figure 4 (c) and (d) we present the dependence of the output frequency shift ω_{out} from the unperturbed $^3P_0 \rightarrow {}^1S_0$ transition frequency as a function of the cavity detuning δ. This is plotted for different values of the balance parameter b and for different static magnetic field strengths B. One may see that the sensitivity of the output frequency to the balance parameter b decreases approximately twice when B increases twice, from 0.05 G to 0.1 G. We expect that by increasing the magnetic field B to a few G, the sensitivity of the output frequency to the balance parameter b can be made less than 1 mHz per 10% imbalance.

Simulations were performed using the computer algebra system "Wolfram Mathematica" [15], and the programming language "Julia" [16].

IV. Conclusion

The creation of continuously-operating bad-cavity lasers on the $^3P_0 \rightarrow {}^1S_0$ transition in ultracold strontium has become possible with the emergence of high-flux sources of ultracold strontium atoms. Replenishing the ultracold atoms in the cavity can be achieved using an optical conveyor at a magic wavelength. An optical conveyor propagating along a ring cavity offers a number of advantages compared with schemes in which the optical conveyor crosses a cavity with a standing wave magic optical lattice. A ring geometry allows greatly increased conveyor speeds reducing atom losses and decreasing the density of the atoms. ^{88}Sr is attractive due to its high abundance and because the absence of hyperfine structure makes it easy to manipulate. However, it requires a strong external magnetic field to allow the $^3P_0 \rightarrow {}^1S_0$ transition. This field causes shifts. We showed that for a 200 G bias magnetic

field B, the inhomogeneity on the level of 75 mG over the active path of the conveyor is sufficient to prevent superradiant lasing because the radiating dipoles cannot synchronize. More problematically, variations in the strength of this external magnetic field will cause shifts in the clock transition frequency of 93 mHz/mG. By contrast, in ^{87}Sr the transition is slightly allowed. At moderate (~1G) values of external static magnetic field B it becomes possible to simultaneously lase on two stretched transitions, with $m = \pm 9/2$, in a non-synchronized regime, producing two-frequency output radiation. In this case the arithmetic mean of these two frequencies will be immune to fluctuations of the magnetic field from the linear Zeeman effect. Population imbalance on two stretched transitions may shift this mean frequency line, however, its role decreases with increasing Zeeman splitting between the stretched transitions and at field strengths of ~1G mHz stability appears possible.

ACKNOWLEDGMENT

The work was supported by the European Union Horizon 2020 research and innovation programme, Quantum Flagship project No 820404 “iqClock”, and No 860579 “MoSaiQC”.

REFERENCES

[1] E. Oelker, R. B. Hutson, C. J. Kennedy, L. Sonderhouse, T. Bothwell, A. Goban, D. Kedar, C. Sanner, J. M. Robinson, G. E. Marti, D. G. Matei, T. Legero, M. Giunta, R. Holzwarth, F. Riehle, U. Sterr, J. Ye, “Demonstration of 4.8×10^{-17} stability at 1 s for two independent optical clocks,” Nature Photonics, vol. 13, pp. 714-719, 2019.

[2] D. Meiser, J. Ye, D. R. Carlson, and M. J. Holland, “Prospects for a millihertz-linewidth laser,” Phys. Rev. Lett., vol. 102, p. 163601, 2009

[3] J. Chen, “Active optical clock,” Chin. Sci. Bull. vol. 54, pp. 348-352, 2009.

[4] M. A. Norcia, J. R. K. Cline, J. A. Muniz, J. M. Robinson, R. B.Hutson, A. Goban, G. E. Marti, J. Ye, J. K. Thompson, “Frequency Measurements of Superradiance from the Strontium Clock Transition,” Phys. Rev. X, vol. 8, p. 021036, 2018.

[5] G. A. Kazakov and T. Schumm, "Active optical frequency standards using cold atoms: Perspectives and challenges," *2014 European Frequency and Time Forum (EFTF)*, 2014, pp. 411-414.

[6] S. Bennets, C.-C. Chen, B. Pasquiou, F. Schreck, “Steady-State Magneto-Optical Trap with 100-Fold Improved Phase-Space Density,” Phys. Rev. Lett., vol. 119, p. 223202, 2017.

[7] C.-C. Chen, S. Bennetts, R. G. Escudero, B. Pasquiou, F. Schreck. Continuous Guided Strontium Beam with High Phase-Space Density. Phys. Rev. Applied, vol. 12, p. 044014, 2019.

[8] R. G. Escudero, C.-C. Chen, S. Bennetts, B. Pasquiou, Florian. Schreck, “A steady-state magneto-optical trap of fermionic strontium on a narrow-line transition,” eprint arXiv:2104.06814, 2021.

[9] J.R. Cline, D. Young, V. M. Schäfer, and J. K. Thompson, “Continuous loading and transport of strontium atoms in a ring cavity”. 52nd Annual Meeting of the APS Division of Atomic, Molecular and Optical Physics, online, May 31 -- June 04, 2021.

[10] A. V. Taichenachev, V. I. Yudin, C. W. Oates, C. W. Hoyt, Z. W. Barber, L. Hollberg, “Magnetic Field-Induced Spectroscopy of Forbidden Optical Transitions with Application to Lattice-Based Optical Atomic Clocks,” Phys. Rev. Lett., vol. 96, p. 083001, 2006.

[11] Ch. Lisdat, J. S. R. V. Winfred, T. Middelmann, F. Riehle, U. Sterr, “Collisional Losses, Decoherence, and Frequency Shifts in Optical Lattice Clocks with Bosons,” Phys. Rev. Lett. vol. 103, p. 090801, 2009.

[12] M. M. Boyd, “High Precision Spectroscopy of Strontium in an Optical Lattice: Towards a New Standard for Frequency and Time,” PhD thesis, University of Colorado Boulder, 2007.

[13] X. Zhang, M. Bishof, S. L. Bromley, C. V. Kraus, M. S. Safronova, P. Zoller, A. M. Rey, J. Ye, “Spectroscopic observation of SU(N)-symmetric interactions in Sr orbital magnetism,” Science, vol. 345, pp. 1467 - 1473, 2014.

[14] M. J. Martin, M. Bishof, M. D. Swallows, X. Zhang, C. Benko, J. von-Stecher, A. V. Gorshkov, A. M. Rey, Jun Ye, “A Quantum Many-Body Spin System in an Optical Lattice Clock,” Science, vol. 341, pp. 632 - 636, 2013.

[15] M. Bishof, M. J. Martin, M. D. Swallows, C. Benko, Y. Lin, G. Quemener, A. M. Rey, J. Ye, “Inelastic collisions and density-dependent excitation suppression in a ^{87}Sr optical lattice clock, Phys. Rev. A, vol. 84, p. 052716, 2011.

[16] Wolfram Research, Inc., Mathematica, Version 11.3.0.0.

[17] J. Bezanson, S. Karpinski, V. B. Shah, A. Edelman, “Julia: A fast dynamic language for technical computing,” eprint arXiv:1209.5145, 2012.